Deformation measurement of a driven pile using distributed fibre-optic sensing

C. Monsberger [1)], H. Woschitz [1)], M. Hayden [2)]

[1)] Institute of Engineering Geodesy and Measurement Systems, Graz University of Technology, Steyrergasse 30, 8010 Graz, Austria
[2)] Keller Grundbau GmbH, Mariahilfer Straße 127a, 1150 Vienna, Austria

Abstract. New developments in distributed fibre-optic sensing allow the measurement of strain with a very high precision of about 1 µm/m and a spatial resolution of 10 millimetres or even better. Thus, novel applications in several scientific fields may be realised, e.g. in structural monitoring or soil and rock mechanics. Especially due to the embedding capability of fibre-optic sensors, fibre-optic systems provide a valuable extension to classical geodetic measurement methods, which are limited to the surface in most cases.

In this paper, we report about the application of an optical backscatter reflectometer for deformation measurements along a driven pile. In general, pile systems are used in civil engineering as an efficient and economic foundation of buildings and other structures. Especially the length of the piles is crucial for the final loading capacity. For optimization purposes, the interaction between the driven pile and the subsurface material is investigated using pile testing methods. In a field trial, we used a distributed fibre-optic sensing system for measuring the strain below the surface of an excavation pit in order to derive completely new information.

Prior to the field trial, the fibre-optic sensor was investigated in the laboratory. In addition to the results of these lab studies, we briefly describe the critical process of field installation and show the most significant results from the field trial, where the pile was artificially loaded up to 800 kN. As far as we know, this is the first time that the strain is monitored along a driven pile with such a high spatial resolution.

Keywords. fibre-optic deformation measurement, optical backscatter reflectometer, distributed sensing, driven pile, soil mechanics

1 Introduction

In civil engineering, piles are widely used if the soil conditions are poor (e.g. soft soil) to form a proper foundation for heavy structures like buildings. The length of the piles depends on the soil conditions. Basically, the lower end of the pile (toe) needs to reach a stable, load-bearing soil layer.

The bearing capacity of a pile depends on the toe resistance σ_s and the shaft friction τ_m along the pile and is determined by a conventional static load test. Unfortunately the result is a combination of both, σ_s and τ_m. A new bidirectional static load test (″Pile HAY-Proof-System®″, invented in 2008, Hayden and Kirchmaier, 2010) overcomes this limitation and allows to separate the two main parts of bearing capacity, σ_s and τ_m.

But even there, the measured shaft friction τ_m is an average value, although it varies along the pile in dependence on the conditions of the different soil layers in reality. It is state of the art to measure the time spans that are needed for driving the pile in one meter steps and to use this information, as well as experience, to distribute the measured shaft friction along the shaft and thus relates it to certain soil layers.

With the variation of τ_m along the pile, different parts of the pile should show different strain values. Thus, strain measurements along the pile may be used to do an enhanced determination of shaft friction along the pile. It is not possible to do these measurements, especially with a sufficient spatial resolution (some cm), using traditional strain gauges for example, because of difficult cabling issues (lack of space for hundreds of cables), the fragility of the strain gauges and the lack of time to apply them to the pile during the construction process.

A distributed fibre-optic system is advantageous against these sensors as there is only one lead-in cable necessary. However, as the sensor elements (glass fibre) are also fragile, a proper installation technique has to be found, which fits to the construction process of the pile.

In the following, we give a brief introduction about pile construction and pile testing, discuss the basic principles of a suitable distributed fibre-optic measuring system and show the setup of the sensing fibre. Afterwards, we show the capabilities of the system by means of results of laboratory testing and by the results of a field trial with an instrumented pile.

2 Pile construction

As an example, the production of Keller Ductile Piles (KDP) piles will be described. They are made of ductile cast iron or steel ST52 and pushed into the ground using a hydraulic quick impact hammer (fig.1 and fig.2). The first pile element (e.g. 5 m length, ∅ 118 mm, 7,5 mm wall thickness) is equipped with a driving shoe (fig.1a), which has a diameter that is slightly larger than the one of the pile.

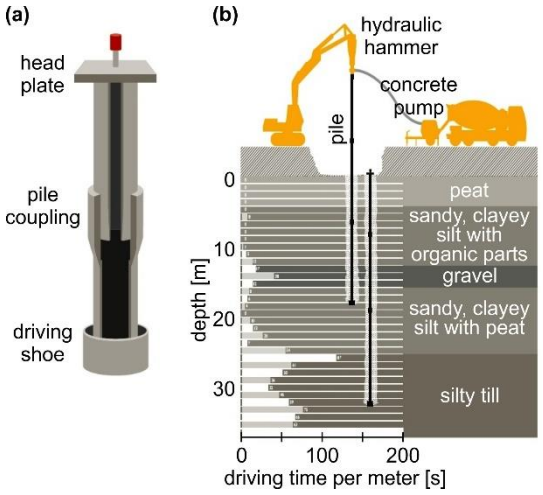

Fig. 1 (a) Schema of a KDP (Keller Ductile Pile) pile and (b) a pile whilst the driving process, showing the dependency of the driving time on the bearing capacity of different soil layers

While driving, grout is inserted into the cavity that is formed by the driving shoe by compressing the surrounding soil material. Later, when hardened, grout provides a connection between the soil and the pile and thus contributes to the bearing capacity of the pile. After one pile element is driven into the soil, the next element is inserted into the conical collar at its upper end. Later, the hydraulic hammer impacts cause a friction-type connection between the two elements.

The pile is driven down to the required final depth, until it reaches a load-bearing soil layer (e.g. silty till, fig.1b). Currently, the depth of this load-bearing soil layer is determined by measuring the penetration speed of the pile during driving.

Later, when load is applied to the pile, it is transferred to the soil, and the bearing capacity of the pile depends on both, the shaft friction and the toe resistance. Both quantities strongly depend on the local soil conditions.

Fig. 2 (a) Pile during construction and (b) detail of a pile with ∅ 118 mm with surrounding material

3 Static load test using the Pile HAY-Proof-System®

On a construction site several 100 of piles may be installed. In advance, static load tests of a few piles may be performed to optimize the pile length and to proof bearing capacity. Several setups are known (see e.g. England, 2008 or Osterberg, 1998), among them the ″Pile HAY-Proof-System®″ (Hayden and Kirchmaier, 2010) which is advantageous against others because of its rather simple setup, fig.3.

Immediately after constructing the pile, when the grout is still soft, a tension pipe (1), which ranges down to the lower end of the pile, is installed. There it is placed on the base cap (5) and thus forms a force-bearing connection between the grouting suspension, the load bearing element (usually ductile pipe) and the tension pipe (1).

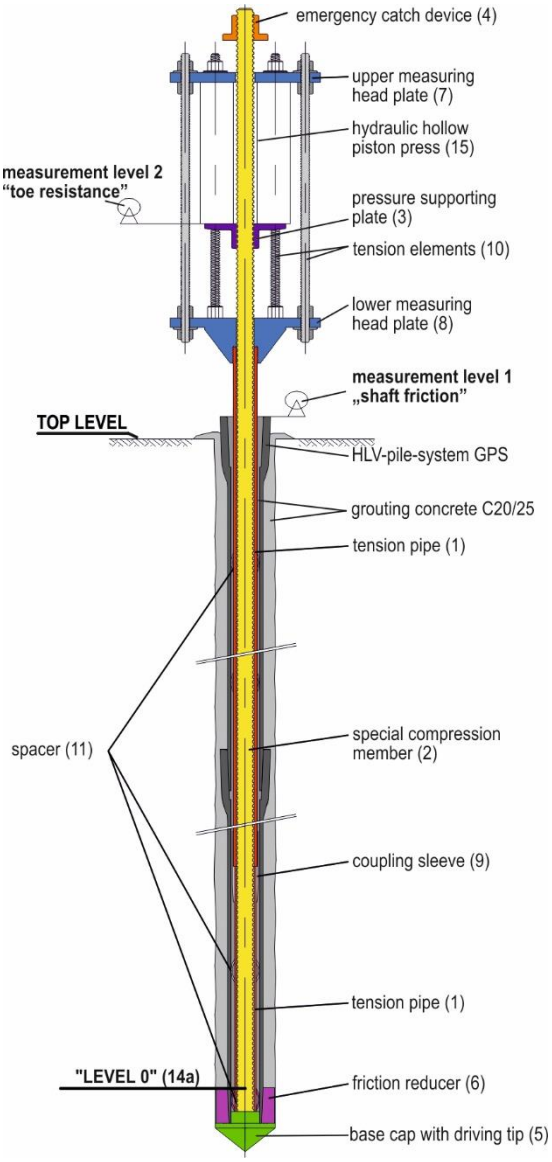

Fig. 3 Schema of the Pile HAY-Proof-System®
with a KDP pile

The tension pipe (1) is used to transfer and distribute the tensile forces along the entire pile length. This pipe also serves as a sleeve for a special compression member (2). A height-adjustable pressure supporting plate (3) is mounted on the upper end of the compression member (2) by means of a special threaded bolt to apply pressure force to the compression member. In addition, an emergency catch device (4) is provided on the upper end of the compression member (2) by means of a special nut for additional safety. Coupling sleeves (9) are used to elongate the tension pipe (1) to the length needed. For the proper centring of the tension pipe, special spacers (11) are used.

In this test system, the base cap or driving tip (5) serves as an abutment together with the surrounding soil. In order to avoid bonding between base cap, concrete and pile pipe, textiles are placed as ″friction reducers″ (6) in the base cap region.

The upper end of the Pile HAY-Proof-System® is the so-called measuring head. It comprises the upper (7) and lower measuring head plates (8) and six tension elements (10) with their nuts.

Principle

Regarding to the flow of forces, the upper measuring head plate (7) serves as an abutment for the hydraulic press (15), which applies the forces (see fig.4). The lower measuring head plate (8) is force-locked to the tension pipe (1) by means of a special threaded bolt. Pressure reaction force is transferred to the lower measuring head plate (8) and thus into the tension pipe (1) via the upper measuring head plate (7) and the six tension elements (10).

The pressure force is now applied to the compression member (2) via a pressure supporting plate (3) and transferred to a special reinforced base cap (5) or load distribution plate (12a) without any significant friction loss.

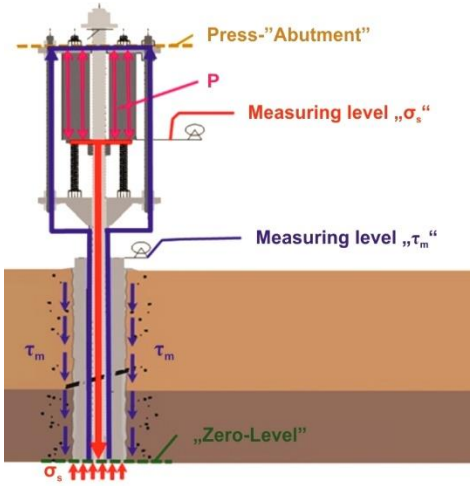

Fig. 4 Function of Pile HAY-Proof-System®

The pipe geometry (grouting) for measuring the outer load bearing capacity is the same as in building piles.

It is one of the advantages of the test method, that due to the bidirectional action, only about half of the

pressure force of conventional pile load tests needs to be applied to the pile head in order to yield comparable test pile reactions.

Result of the test

During the test the applied force is increased until the pile fails, which is determined by measuring the pile deformation at the two measuring levels (see fig.4) with LVDT sensors. Thus one gets the so-called ultimate load from shaft friction (e.g. 800 kN) and toe resistance (e.g.120 kN) as a result of the pile test.

But there is still the drawback, that one does not know the proportion of the shaft friction distribution in the different soil layers, which is important for optimization of the pile length.

This is why we investigated, if it is possible to extend the system by fibre-optic measurements, which should gather information about the tensions along the pile shaft during the pile test. By this, one might be able to determinate the shaft friction from each layer along the whole pile shaft with our driving criteria.

4 Fibre-optic measuring system

Rayleigh scattering is one of the major effects causing intensity loss in optical fibres. It is caused by variations of the refractive index profile along the fibre core and effects about 85% of the natural attenuations, see e.g. Wuilpart (2011). In general, the Rayleigh scatter amplitude has a random but static behaviour along the fibre. External influences, like changes in strain or temperature, cause a spectral shift in the local reflected Rayleigh pattern. Therefore, a small, local segment of the fibre can be interpreted as a weak reflecting fibre Bragg grating with a random period. Furthermore, the modelling of the distributed measurement system can be realised by splitting the fibre in equidistant segments and calibrating the local respective Rayleigh shift in reference to changes in strain or temperature.

In the present application, we used an optical backscatter reflectometer (OBR). The interrogation unit is able to record sensing information with a very high resolution of about ±1.0 µm/m for strain and about ±0.1°C for temperature measurements (Luna, 2014a). Moreover, a spatial resolution of about 10 millimetres or even better may be realised. The measurement principle is based on the optical frequency domain reflectometry (OFDR) technique. Thereby, the Rayleigh backscatter amplitudes and phases are recorded in the frequency domain. Then, the signal, as a function of the fibre length (equivalent to the classical optical time domain reflectometry, OTDR), is obtained through a Fourier transformation. For details on the optical network and the measurement principle see Soller et al. (2005) or Kreger et al. (2006).

In order to form a distributed measurement system, the Rayleigh backscatter of the sensing fibre is recorded in a known strain and temperature state. This initial measurement can be interpreted as a reference scan. Later, the fibre is scanned again, when the strain and/or the temperature state has changed. Then, the signals of both measurements are divided in equidistant segments, where the length of the segment Δz corresponds to the spatial resolution of the OBR. To determine the external influences, the spectrum of each segment is observed in the frequency domain. Because of the changed strain and/or temperature state, a spectral shift arises between the reference and the influenced scan. The size of the shift can be calculated by performing a cross correlation between the two spectra. By this, for each segment of the sensing fibre, it is possible to realize a distributed measurement system.

Fig.5a shows the wavelength spectrum of an interval with a length of $\Delta z = 10$ mm for an unstrained reference scan and the spectra of the same segment of the fibre with an applied strain of about 1000 µm/m. The cross correlation between the two spectra can be seen in fig.5b. Thereby, the resulting wavelength shift, $\Delta\lambda$, is directly proportional to the apparent strain in this fibre segment.

In civil engineering, applications in harsh environments are prevalent. Therefore, a robust sensor cable is required to protect the optical sensor during the field instrumentation and monitoring. In our project, the strain sensing cable BRUsens strain V4 from Brugg Cables was used, which has an outer diameter of about 3 mm. Its basic setup is shown in fig.6. A metal tube protects the glass fibre and thus makes the cable robust. For strain sensing it is important that all layers of the cable are interlocking and ensure a proper strain transfer to the sensing fibre core. The manufacturer guarantees an operating strain range of 10 000 µm/m (Brugg, 2012).

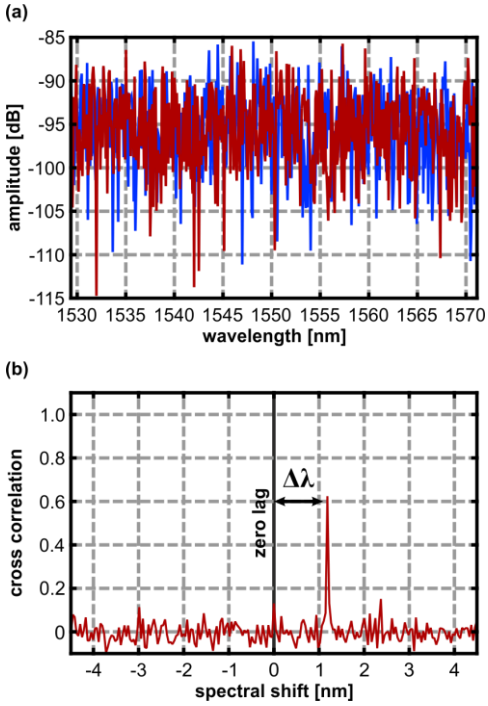

Fig. 5 (a) Wavelength spectrum for an unstrained (blue) and a strained (red) fibre segment of 10 mm length and (b) the corresponding cross correlation function

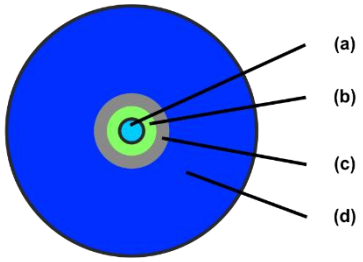

Fig. 6 Structure of the sensing cable BRUsens strain V4; (a) strain sensing single mode fibre (∅ 250 µm); (b) multi-layer buffer with strain transfer layer; (c) metal tube for protection; (d) polyimide outer sheath

5 Calibration of the fibre-optic measuring system

Many manufactures do not specify individual calibration parameters for their fibre-optic sensors, but refer to literature values without further information. However, using standard values might result in errors of up to 10% (Luna Technologies 2014b). By individual calibration, one can avoid these errors and thus, calibration is essential when a reliable fibre-optical monitoring system is needed.

5.1 IGMS calibration device for fibre-optic strain sensors

For the calibration and testing of FO strain sensors we have developed a unique facility within the last years. It allows the fully automatic calibration of sensors with a maximum length of 30 m without folding. Key components are a linear translation stage which allows a maximum sensor elongation of 300 mm and a laser interferometer as a reference measurement system. For details, reference is given to Woschitz et al. (2015).

The accuracy of the facility depends on the sensor length and the maximum strain applied to it. For example, for a 5 m long strain sensor, which is strained for 30 000 µm/m, the expanded standard uncertainty of the reference system (determined in accordance to ISO/BIPM, 1995) is about $U_{\Delta L} = \pm 2.5$ µm ($k = 2$) which corresponds to an expanded standard uncertainty in strain of about $U_{\varepsilon} = \pm 0.5$ µm/m.

5.2 System calibration

As discussed above, the local Rayleigh shift between a reference epoch and subsequent measurements depends on both, strain ε and temperature changes ΔT. The transfer from the measured wavelength shift Δλ [nm] or the frequency shift Δν [GHz] to these quantities can be approximated by the linear function

$$\frac{\Delta\lambda}{\lambda} = \frac{-\Delta\nu}{\nu} = K_{\varepsilon}\,\varepsilon + K_T\,\Delta T \qquad (1)$$

with the normalized sensitivity coefficients K_{ε} and K_T and the centre wavelength λ, or the centre frequency ν, of the scan. Thereby, this equation is identically to the response of a fibre Bragg grating, see Soller et al. (2006). Assuming that the sensing fibre exhibits no strain or is on constant temperature, the linear function can be split and written as:

$$\frac{\Delta\lambda}{\lambda} = \frac{-\Delta\nu}{\nu} = K_{\varepsilon}\,\varepsilon\Big|_{\Delta T=\text{const.}}$$
$$\frac{\Delta\lambda}{\lambda} = \frac{-\Delta\nu}{\nu} = K_T\,\Delta T\Big|_{\varepsilon=\text{const.}} \qquad (2)$$

For the determination of K_{ε}, we used a 2 m long sample of the sensing cable (same as used at the pile) using our calibration device in the laboratory.

Regarding our experience, we applied a pre-strain of about 800 µm/m to the fibre, in order to avoid nonlinearities in the low strain region. We then strained the fibre in three full cycles for another 2500 µm/m, using steps of 100 µm/m.

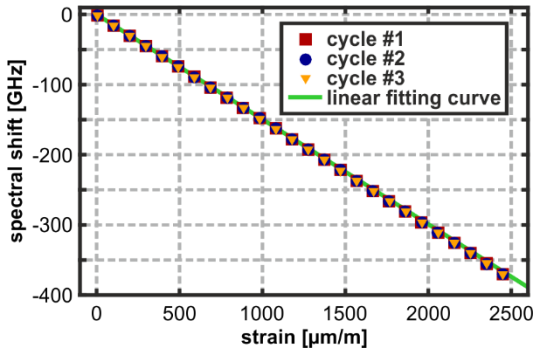

Fig. 7 Measurement results of strain calibration and linear fitting curve

Fig.7 shows the measured spectral shift of the interrogation unit in relation to the true strain values provided by the calibration device. The results of all cycles coincide well with a maximum deviation of about 0.6 GHz (≈ 4 µm/m). For this application, it is sufficient to assume linear behaviour when estimating the strain coefficient.

The cable manufacturer does not provide sensing parameters for Rayleigh backscattering systems. However, using a literature value - these vary in recent literature from 0.7314 (SMF 28e fibres, Kreger et al. 2009) to 0.780 (standard germanium-doped silica fibres, Luna 2014b) - instead of the value estimated by us ($K_\varepsilon = 0.7733$), might result in an error of the derived strain values of about 5%.

For our application, the temperature sensitivity of the fibre can be neglected as the fibre-sensor will be vertically embedded into the soil and the temperatures remain almost constant during the period of pile testing. Else, the temperature effects might be eliminated using the results of an unstrained temperature sensing fibre which is installed nearby the strain sensing fibre.

6 Field trial

6.1 Instrumentation

Up to now, it was not known whether or not a sensing fibre made from glass can survive the harsh pile installation process. There, accelerations of more than 1800 g act on the pile during the driving process generated, by the hydraulic hammer, and loose gravel (stones) may break the fibre cable.

By evaluating several possible installation techniques, we finally decided to use a specific type of collar clamp to attach the fibre to the pile. In laboratory investigations we found, that a spacing of 1 m between the clamps is sufficient to properly connect the fibre to the pile.

Finally, in a first field trial we installed a sensing fibre to a 15 m long pile (fig.2). Despite the results in the lab, we have chosen a smaller spacing (0.5 m) in the critical lower region of the pile.

The pile elements were 5 m long and thus the fibre passes two pile couplings with its conical collars (see sect.2). Although the fibre was protected in these two sections, it broke at the lower pile coupling and thus, later the deformation could only be measured on the upper, 9 m long, section of the pile.

6.2 Fibre-optic measurements during the static load test of the pile

During testing the pile with Pile HAY-Proof-System®, a set of forces is applied to the pile. During a primary test, the toe resistance σ_s and shaft friction τ_m is determined simultaneously. After the failure of the toe resistance σ_s, a secondary test is performed to get the ultimate load of the shaft friction τ_m (see sect.3 for the setup). Fig.8 shows the applied loads which basically were increased in steps of 100 kN. However, to allow the pile to get on tension, the first load step is smaller (20 kN).

In the primary test, the soil beneath the base cap failed while increasing the force applied to the compression member from 100 to 200 kN, at a load of approx. 120 kN, which results in a toe resistance σ_s of about 3.87 MN/m^2.

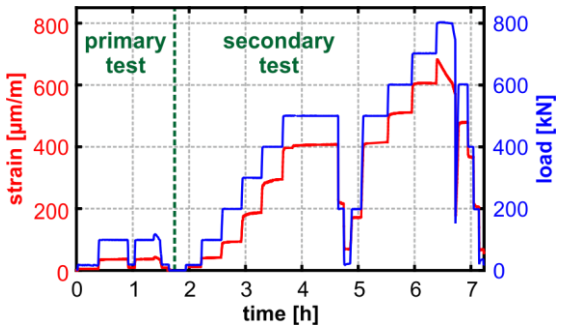

Fig. 8 Applied load (blue) and mean measured strain (red) during static pile testing in the field

Afterwards, the setup was modified (see sect.3) and the applied force was increased step-wise, first up to 500 kN, and after a short releasing period further on up to 800 kN. The short releasing periods are necessary to determine hysteresis effects.

Whilst the whole load test, data were acquired continuously (sampling frequency of about 0.1 Hz) with the fibre-optic measuring system. The raw values were converted using the strain sensitivity coefficient determined in sect.4.2.

For a first evaluation, the average strain over the upper section of the pile (i.e. 9 m long measurement fibre) was computed for every measurement epoch. These values are also depicted in fig.8 and by this it is evident, that the strain increases with applied load. However, creepage arises in the beginning of a load step, and usually stabilizes after some minutes. Then, at 800 kN (at approx. 400 min), the shaft friction failed to withstand the applied force and the pile was pulled out of the soil for some centimetres.

6.3 Results

In this section, some results are discussed in order to demonstrate the capabilities of the fibre-optic system under field conditions.

First, in order to discuss precision, 10 consecutive measurements are plotted in fig.9. In the abscissa, 0 m represents the earth's surface. The measurements were gathered at the end of one load step (100 kN), where creepage is minimal. The signals of all 10 measurements lie upon each other and show only a minimal trend, which is induced by the chosen reference measurement and the still emerging minimal creepage.

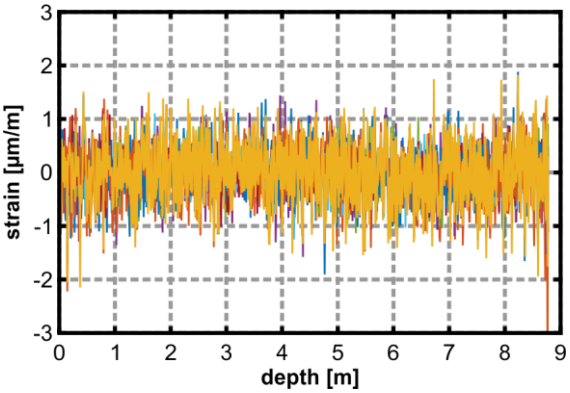

Fig. 9 Result of 10 consecutive strain measurements at an applied load of 100 kN

The noise of all signals is rather low with a maximum standard deviation of $\sigma_\varepsilon \approx 0.5$ µm/m. Tests in the laboratory have shown almost the same values, indicating that the location of the interrogation unit in the field (inside a container) and the protection of the lead-in fibre are appropriate for precise measurements.

Fig.10 shows strain measurements at all load steps of the primary test. The reference measurement was gathered at 0 kN load. The strain varies slightly along the pile (6 - 17 µm/m) at 20 kN, except the larger peak (45 µm/m) at a depth of 2.6 m. This peak gets more significant, after increasing the load to 100 kN. From a ground-opening close by it is known that a different soil layer starts at approx. this depth, which is assumed to cause this conspicuous strain behaviour.

At the top of the pile, above of the first clamp (positions of the clamps are indicated in fig.10 by the gray dashed lines), the fibre does not have any connection to the pile and thus, there emerges no strain.

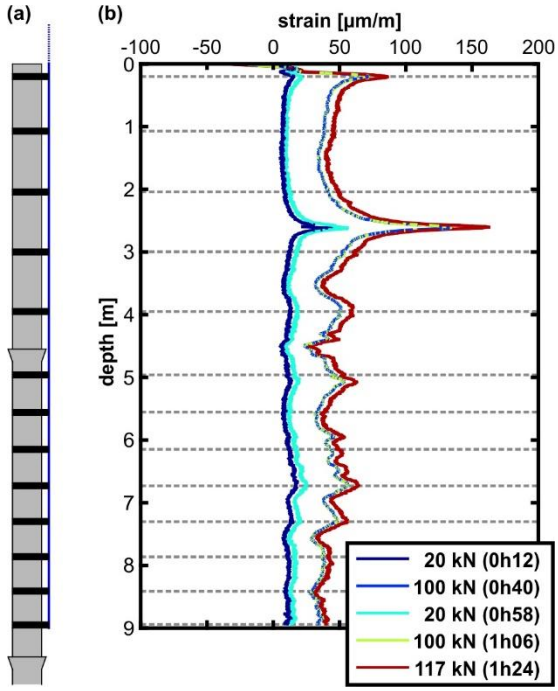

Fig. 10 (a) Schema of the upper two pile elements with the location of the clamps (black) and
(b) the measured strain profiles along the pile at selected time intervals of the load steps of the primary test

After the first increase of load, it was lowered to 20 kN and then increased again to 100 kN. Fig.11

shows the hysteresis in the strain values after lowering the load at the 20 kN load step. The pile remains slightly on strain, on average about 4 µm/m with minor variations. A higher strain level (about 24 µm/m) reveals the interface between the two soil layers (2.6 m depth), which can also be seen as a small discontinuity (up to 3.5 µm/m) in the difference of the two measurements at 100 kN load. But except this small discontinuity, there is absolutely no hysteresis apparent at the 100 kN load step. This may be explained by the fact, that 100 kN was the maximum load applied to the pile up to this moment. Except the discontinuities, the maximum difference between the two signals at 100 kN is less than 1 µm. This is astonishing, as there is a time span of 25 min and a load change in between the two measurements.

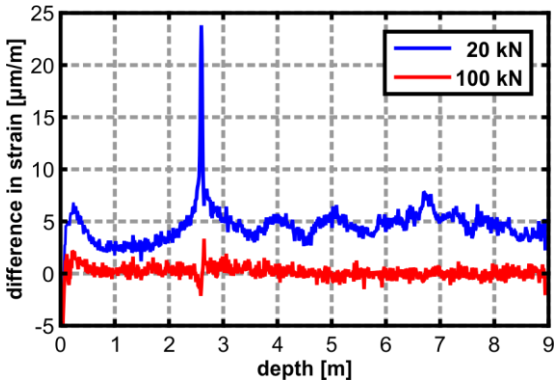

Fig. 11 Strain differences at the two different loads of the repeated loadings of the primary test

Now we want to focus on another interesting phenomenon, which is well known in civil engineering: the evolution of cracks in the grouting material. But, to our knowledge, it was not measured as precisely before on a driven pile and thus was not studied in great detail. Fig.12 shows a series of strain profiles at different loads and time. Fig.12a shows the strain values along the pile at a load of 200 kN. There are no cracks visible, only the large strain at 2.6 m depth (different soil layers) and the strain decrease at the top of the pile (above the first clamp, fibre not connected to the pile) attract attention. Little later, when increasing the load, the first crack arises at about 260 kN, fig.12b. The arising cracks are numbered in fig.12, and major cracks are highlighted in red. Due to the crack, the tensile strength of the pile decreases in the region of the crack and thus the strain increases, in the case of crack #1 for about 310 µm/m. Little below, another crack (#2) opens slightly (strain increase of 56 µm/m), but remains constant in width for another 90 seconds. Then, the crack opens suddenly and causes an increase in strain of about 640 µm/m (fig.12e). The position of this crack is close to the first pile coupling and thus a relationship between the two might be evident. Anyway, in this region the stiffness of the pile is different compared to the other regions because of the larger diameter of the conical collar.

In the time in between these 90 s, another 6 cracks (#3 - #8) appear, with different strain amplitudes. Later, with increasing force (not shown here) the smaller cracks open further and many more new cracks appear.

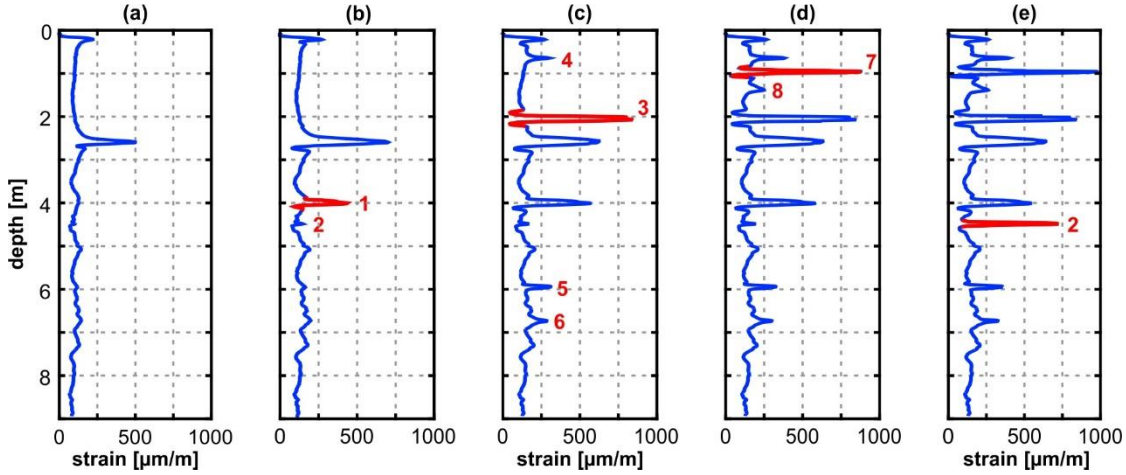

Fig. 12 Strain profile along the pile during the secondary test at a load of (a) 200 kN (t= 2h56m00s), (b) 260 kN (t= 2h56m30s), (c) 300 kN (t= 2h57m00s), (d) 300 kN (t= 2h57m30s) and (e) 300 kN (t= 2h58m00s)

7 Conclusion

During the field measurements, the distributed fibre-optic measuring system (OBR) has shown excellent performance with a precision of less than 1 µm/m in strain measurement.

Although the chosen sensing fibre with its metallic tubing is relatively robust compared to other fibre types, the fibre broke whilst driving the pile due to the harsh conditions and part of the measuring fibre was lost in the field trial. As a consequence, a more robust type of fibre-optic sensing cable is indispensable when instrumenting a driven pile. However, in this first trial a more robust sensor cable was not used because of its higher tensile strength.

Despite of this inconvenience in the field trial, we could proof that using fibre-optic sensors in such a harsh environment is not a hopeless intension and even the first results have revealed information that that cannot be measured using other techniques.

It is planned to continue the development in future. By combining fibre-optic measurements with the Pile HAY-Proof-System®, we hope to get a powerful tool, which can be used for proper correlating driving criteria to the shaft friction distribution and this will finally result in optimized pile production techniques.

Acknowledgements

We would like to thank the companies Keller Grundbau GmbH (Dr. V. Racansky) for the opportunity to realize this project, and Brugg Cables AG for their support.

References

Brugg (2012). Data Sheet: BRUsens strain V4. Vers. 2012/06/19 Rev. 01 TH, Brugg Cables AG, Brugg, CH, 1p.

England, M. (2008). Review of methods of analysis of test results from bi-directional static load tests. Proc. 5th Int. Symp. on Deep Foundations on Bored and Auger Piles (BAP V), Ghent, Belgium, 5 p.

Hayden, M. and Th. Kirchmaier (2010). Pile HAY-Proof-System® (Pile H-P-S) – Neuartiges System für statische Probebelastungen an schlanken Pfählen. Proc. 25th Christian Veder Colloquium, Graz University of Technology, 22 p.

ISO/BIPM (1995). Guide to the Expression of Uncertainty in Measurement, International Organisation of Standards, Switzerland.

Kreger, S.T., D.K. Gifford, M.E. Froggatt, B.J. Soller and M.S. Wolfe (2006). High resolution distributed strain or temperature measurements in single-and multi-mode fiber using swept-wavelength interferometry. In: *Optical Fiber Sensors*, Optical Society of America, Washington DC, USA, pp. ThE42

Kreger, S.T., A.K. Sang, D.K. Gifford and M.E. Froggatt (2009). Distributed strain and temperature sensing in plastic optical fiber using Rayleigh scatter. In: *SPIE Defense, Security and Sensing*, International Society for Optics and Photonics, Bellingham, USA, pp. 73160A-73160A

Luna (2014a). Data Sheet: Optical Backscatter Reflectometer (Model OBR 4600). Ver. LTOBR4600 REV. 004 02/13/2014, Luna technologies Inc., Roanoke, USA, 1p.

Luna (2014b). User Guide: Optical Backscatter Reflectometer Model OBR 4600. Ver. User Guide 5, OBR 4600 Software 3.6, Luna technologies Inc., Roanoke, USA, 230p.

Osterberg, J.O. (1998). The Osterberg Load Test Method for Drilled Shafts and Driven Piles – The First Ten Years. 7th Int. Conf. and Exhibition on Piling and Deep Foundations, Vienna, Austria, 17 p.

Soller, B.J., M.S. Wolfe and M.E. Froggatt (2005). Polarization resolved measurement of Rayleigh backscatter in fiber-optic components. OFC Technical Digest, paper NWD 3, Los Angeles, USA, 6 p.

Wuilpart M. (2011). Rayleigh scattering in optical fibers and applications to distributed measurements. In: *Thévanez, L. (ED.), Advanced Fibre Optics: Concepts and Technology*, EPFL Press, Lausanne, CH, pp. 207-262

Woschitz, H., F. Klug and W. Lienhart (2015). Design and calibration of a fiber optic monitoring system for the determination of segment joint movements inside a hydro power dam. IEEE J. of Lightwave Tech.33, Issue 12: 2652-2657